UvA-DARE (Digital Academic Repository)

Strigolactones regulate sepal senescence in Arabidopsis

Xu, X.; Jibran, R.; Wang, Y.; Dong, L.; Flokova, K.; Esfandiari, A.; McLachlan, A.R.G.; Heiser, A.; Sutherland-Smith, A.J.; Brummell, D.A.; Bouwmeester, H.J.; Dijkwel, P.P.; Hunter, D.A.

Link to publication

RESEARCH PAPER

Strigolactones regulate sepal senescence in Arabidopsis

Xi Xu[1,2], Rubina Jibran[2], Yanting Wang[3], Lemeng Dong[3], Kristyna Flokova[3], Azadeh Esfandiari[2],
Andrew R.G. McLachlan[2], Axel Heiser[4], Andrew J. Sutherland-Smith[1], David A. Brummell[2],
Harro J. Bouwmeester[3], Paul P. Dijkwel[1,*] and Donald A. Hunter[2,*]

[1] Massey University, School of Fundamental Sciences, Palmerston North, New Zealand.
[2] The New Zealand Institute for Plant and Food Research Limited, Private Bag 11600, Palmerston North 4442, New Zealand
[3] Swammerdam Institute for Life Sciences, University of Amsterdam, Amsterdam, The Netherlands
[4] Hopkirk Research Institute, AgResearch Limited, Palmerston North 4474, New Zealand

* Correspondence: Donald.Hunter@plantandfood.co.nz or P.Dijkwel@massey.ac.nz

Abstract

Flower sepals are critical for flower development and vary greatly in life span depending on their function post-pollination. Very little is known about what controls sepal longevity. Using a sepal senescence mutant screen, we identified two Arabidopsis mutants with delayed senescence directly connecting strigolactones with senescence regulation in a novel floral context that hitherto has not been explored. The mutations were in the strigolactone biosynthetic gene *MORE AXILLARY GROWTH1* (*MAX1*) and in the strigolactone receptor gene *DWARF14* (*AtD14*). The mutation in *AtD14* changed the catalytic Ser97 to Phe in the enzyme active site, which is the first mutation of its kind *in planta*. The lesion in *MAX1* was in the haem–iron ligand signature of the cytochrome P450 protein, converting the highly conserved Gly469 to Arg, which was shown in a transient expression assay to substantially inhibit the activity of MAX1. The two mutations highlighted the importance of strigolactone activity for driving to completion senescence initiated both developmentally and in response to carbon-limiting stress, as has been found for the more well-known senescence-associated regulators ethylene and abscisic acid. Analysis of transcript abundance in excised inflorescences during an extended night suggested an intricate relationship among sugar starvation, senescence, and strigolactone biosynthesis and signalling.

Keywords: Arabidopsis, AtD14, darkness, MAX1, mutants, sepal senescence, strigolactones, sugar starvation.

Introduction

Senescence typically occurs in mature cells of tissues after their growth phase has ceased to enable efficient recycling of nutrients to new growing sinks such as seeds (Thomas, 2013). At the whole–plant level, senescence is considered critical for plant fitness, enabling plants to survive optimally in their given environments. The ability to senesce requires a change in competency of the tissue that happens during ageing (Jing *et al.*, 2005; Fracheboud *et al.*, 2009). Nevertheless, imposition of stress can make tissues senesce early. Prolonged darkness is a stress that results in carbon deprivation and early senescence

of chlorophyllous tissues. This has been observed in individually covered attached leaves (Weaver and Amasino, 2001; Law *et al.*, 2018), and in sepals of immature inflorescences of broccoli and Arabidopsis (Page *et al.*, 2001; Trivellini *et al.*, 2012). Research on the precocious senescence of these tissues has revealed that the signalling key to their degreening is similar to that occurring naturally in leaves *in planta* as they senesce in an age-dependent manner and in response to canopy shading. For example, the phytochrome-interacting factor genes *PIF4* and *PIF5* that have important roles in the shade response of canopy leaves (Sakuraba *et al.*, 2014) were first identified to regulate the precocious degreening of harvested immature inflorescences of Arabidopsis held in the dark (Trivellini *et al.*, 2012). Similarly, mutations in *EIN2* and *ORESARA1/ANAC092* that alter the timing of sepal senescence of dark-held inflorescences (Trivellini *et al.*, 2012) were previously identified in Arabidopsis as components of the feedforward control of age-related leaf senescence (Kim *et al.*, 2009).

Phytohormones have long been known to have key roles in senescence regulation. Ethylene, salicylic acid, abscisic acid, jasmonic acid, and brassinosteroid promote the onset or progression of senescence, whereas cytokinin, gibberellic acid, and auxin delay the process (Gan and Amasino, 1997; Lim *et al.*, 2007). The hormones do not work alone, but rather in concert with each other to control senescence progression. For example, ethylene, abscisic acid, and jasmonates interact to control the timing and progression of leaf senescence in Arabidopsis (Kim *et al.*, 2011).

More recently, strigolactones (SLs), which are well known for their function in regulating seed germination in parasitic plants (Toh *et al.*, 2012; Wang and Bouwmeester, 2018), plant shoot branching (Gomez-Roldan *et al.*, 2008; Umehara *et al.*, 2008), and stress responses such as to drought and high salinity (Bu *et al.*, 2014; Ha *et al.*, 2014), were reported to regulate natural- and dark-induced leaf senescence (Hamiaux *et al.*, 2012; Yamada *et al.*, 2014; Ueda and Kusaba, 2015). SL biosynthesis starts with the conversion of all-*trans*-β-carotene into carlactone (CL), a common precursor of all SLs (Alder *et al.*, 2012; Seto *et al.*, 2014; Wang and Bouwmeester, 2018). In Arabidopsis, this requires the sequential activities of the carotenoid isomerase DWARF27 (D27) and two carotenoid cleavage dioxygenases CCD7/MAX3 and CCD8/MAX4 (Alder *et al.*, 2012). Following this, the MORE AXILLARY GROWTH1 (MAX1) cytochrome P450 monooxygenase (Booker *et al.*, 2005) oxidizes CL into carlactonoic acid (CLA) (Abe *et al.*, 2014), which is further converted by downstream enzymes to other SL-like compounds (Brewer *et al.*, 2016). The bioactive SL is perceived by the D14 receptor, an α/β-fold hydrolase (Arite *et al.*, 2009), which hydrolyses the SL then interacts with the F-box protein MAX2/D3 to trigger SL signalling and response (Yao *et al.*, 2016).

Very little is known about how sepal senescence is regulated, with most research on flowers having focused on petals (Rogers, 2013). To identify key regulators of sepal senescence, we systematically evaluated a population of mutant Arabidopsis plants derived from seeds treated with ethyl methanesulfonate (EMS). By using an Arabidopsis inflorescence degreening assay (Hunter *et al.*, 2018), we previously identified three independent mutations in Chl *b* reductase that resulted in a delayed degreening phenotype (Jibran *et al.*, 2015). Here we report on the characterization of a further two mutants with delayed senescence that highlight the role of SLs in controlling the life span of a floral organ.

Materials and methods

Plant growth conditions and mutant analysis

EMS mutants of *Arabidopsis thaliana* Landsberg *erecta* (L*er*-0) were selected and the causal mutations determined as described in Jibran *et al.* (2015), Hunter *et al.* (2018), Supplementary Fig. S1, and Supplementary Table S1. Mutants were backcrossed twice to wild-type (WT) L*er*-0 prior to analysis and genetic complementation. Seeds were germinated and grown in a temperature-controlled growth chamber set at 21 °C with 65% relative humidity and under a 16 h light (200 μM photons m^{-2} s^{-1}; Gro-Lux and cool-white fluorescent lamps)/8 h dark cycle (long day) unless otherwise stated. For *in planta* assays, plants were grown in a temperature-controlled growth cabinet (Contherm Model CAT 630, Wellington, New Zealand), at 20–22 °C with 60% relative humidity and a 16 h light/8 h dark long-day photoperiod (~180 μE with metal halide lamps). For long-day treatments, inflorescences were placed in a container, covered with transparent film, and incubated in the growth chamber. For SL treatments, inflorescences were treated with the racemic mixture *rac*-GR24, which contains a synthetic SL analogue (Chiralix, Nijmegen, The Netherlands). This was dissolved in pure DMSO and diluted to final concentrations of 5 μM *rac*-GR24 and 1% (v/v) DMSO. Mock treatments for controls were 1% (v/v) DMSO.

Chlorophyll analysis

Chlorophyll (Chl) was extracted from single inflorescences according to Jibran *et al.* (2015) with the following changes: fresh samples were used and samples were incubated in the dark at 4 °C for 4 d after adding ethanol.

RNA isolation and RT–qPCR analysis

Total RNA was isolated from inflorescences using the Quick-RNA™ MiniPrep kit (Zymo Research, Irvine, CA, USA) with on-column DNase treatment. cDNA was synthesized from RNA (500 ng) using iScript™ Reverse Transcription Supermix for quantitative reverse transcription–PCR (RT–qPCR; Bio-Rad, Hercules, CA, USA). The cDNA template was diluted 10 times for RT–qPCR analysis. The RT–qPCR was prepared using a LightCycler® 480 SYBR Green I Master kit (Roche Diagnostics, Mannheim, Germany) and the PCR was performed with a LightCycler® 480 Instrument II (384-well; Roche Diagnostics) on three biological replicates, each with 4–6 pooled inflorescences from individual plants (four technical replicates for each biological replicate). Primers were designed using QuantPrime online software (Arvidsson *et al.*, 2008) and are listed in Supplementary Table S2. The Cp value was calculated using the algorithm of 'Abs Quant/2nd Derivative Max' present in LightCycler® 480 Software (version 1.5). Data were normalized to the reference gene *PP2AA3* (*At1g13320*), which was confirmed to be stable for development and environmental conditions (Czechowski *et al.*, 2005), senescence (Jibran *et al.*, 2015), and SL treatment (Supplementary Fig. S2), and relative transcript abundance changes were calculated using the ΔΔCt method (Livak and Schmittgen, 2001; Dvinge and Bertone, 2009).

nCounter analysis

Transcriptional analysis was performed using the nCounter Analysis System (NanoString, Seattle, WA, USA) (Geiss *et al.*, 2008). Two sets of gene-specific probes (along with a reporter probe and a capture probe) were designed by NanoString Support (see Supplementary Table S3). Total RNA (300 ng) was hybridized using the nCounter PlexSet-24 Reagent Pack according to the 'PlexSet™ Reagents User Manual'. After hybridization, samples were vertically pooled and were placed on the automated nCounter Prep Station (NanoString) for purification and immobilized in the cartridge. This cartridge was then transferred to the nCounter Digital Analyzer for data collection. Data analysis was performed with nSolver™ 4.0 Analysis Software according to the user manual. All samples passed quality control. The background thresholding was set to '12' according to the count value of the internal negative control. Positive control normalization was carried out by using the geometric mean of the top three positive counts. Reference gene normalization was calculated using the geometric mean of counts for the three reference genes *PP2AA3/At1g13320*, *ACT2/At3g18780*, and *MON1/At2g28390* (Czechowski *et al.*, 2005).

In silico analysis

Sequence alignments were performed using Geneious desktop software (Kearse *et al.*, 2012). The three-dimensional (3D) structure of AtD14 was obtained from the SL-induced AtD14–D3–ASK1 complex (PDB: 5HZG) (Yao *et al.*, 2016). The homology model of MAX1 was calculated using the I-TASSER On-line Server (https://zhanglab.ccmb.med.umich.edu/I-TASSER/) (Zhang, 2008; Roy *et al.*, 2010; Yang *et al.*, 2015). The 3D images were prepared with CCP4MG (McNicholas *et al.*, 2011).

Plasmid constructions

For transient expression assays, the Arabidopsis Col-0-based SL biosynthetic genes (*D27*, *MAX3*, *MAX4*, and *MAX1*) were cloned as described in Zhang *et al.* (2014). The L*er*-0-based *MAX1* gene and genetic variants (*MAX1*-WT, *MAX1*-G469R, or *MAX1*-G469A) were cloned using the same protocol but with the primers listed in Supplementary Table S4.

Transient expression in leaves of Nicotiana benthamiana

Enzymatic characterization of MAX1 and the genetic variants was carried out as described in Zhang *et al.* (2014) except that *Agrobacterium tumefaciens* was resuspended in 50 mM MES (Duchefa, Haarlem, The Netherlands)–KOH buffer (pH 5.6) containing 2 mM NaH$_2$PO$_4$ (Merck, Darmstadt, Germany), 100 μM acetosyringone (Sigma-Aldrich, St. Louis, MO, USA), and 0.5% (w/v) glucose (MP Biomedicals, France) to a final OD$_{600}$ of 0.5. Instead of *OsD27*, *OsCCD7*, and *OsCCD8*, we used *AtD27*, *MAX3*, and *MAX4*, which were co-infiltrated with *AtMAX1* and genetic variants to study the conversion of CL to CLA. Infiltration was performed using 4-week-old *N. benthamiana* plants which were soil grown in pots in a plant house with artificial light to make a photoperiod of 16 h light at 25 °C and 8 h dark at 22 °C. For each gene combination, six individual plants were used as biological replicates.

Analysis of carlactone and carlactonoic acid in N. benthamiana

CL and CLA were detected using ultra-high performance-LC-MS/MS (UHPLC-LC-MS/MS) and CLA conjugates with UPLC-LC-quadrupole-time-of-flight-MS (UHPLC-qTOF-MS). For both analyses, 200 mg of fine-ground *N. benthamiana* leaves were extracted in 2 ml of ethyl acetate, using GR24 (5 pmol) as internal standard. Samples were vortexed and centrifuged for 20 min at 2000 *g* at 4 °C. The supernatant was dried *in vacuo*. Prior to mass analysis, samples were reconstituted in

100 μl of 25% acetonitrile/water (v/v) and filtered using a micro-spin 0.2 μm nylon membrane filter (Thermo Fisher Scientific, Waltham, MA, USA).

Targeted analysis of CL and CLA was performed using an Acquity UPLC system (Waters, Milford, MA, USA) coupled to a Xevo® TQ-XS triple-quadrupole mass spectrometer (Waters MS Technologies, Manchester, UK) with electrospray interface. Samples were injected onto a reverse-phase UPLC® Acquity BEH C18 column (2.1×100 mm, 1.7 μm, Waters) at 45 °C. Retention of analytes was controlled by gradient elution of 15 mM formic acid in water (A) and 15 mM formic acid in acetonitrile (B) at a flow rate of 0.4 ml min^{-1}. The 10 min linear gradient started by isocratic elution at 0–0.5 min with 5% B, increased to 60% B in 1.5 min, and to 90% B in the next 5.3 min. The column was washed for 1.5 min with 90% B and equilibrated for initial conditions for 1.5 min. The eluate was introduced in the electrospray interface ion source of the triple quadrupole MS analyser, operating in both positive and negative mode with the following conditions: capillary voltage, 1.2 kV; ion source/desolvation temperature, 150/600 °C; desolvation/cone gas flow, 1000/150 l h^{-1}; cone voltage, 20–25 V; and collision energy, 18–25 eV. MS data were recorded in multiple reaction monitoring mode (MRM) of four characteristic transitions for each of the compounds. The MassLynx™ software package (version 4.2, Waters) was used to operate the instrument, and acquire and process MS data.

Detection and quantification of carlactonoic acid conjugates by UHPLC-qTOF-MS

The *N. benthamiana* leaf extracts were analysed by UHPLC-qTOF-MS consisting of an Agilent 1290 liquid chromatograph coupled to a Bruker Daltonics microTOF-Q mass spectrometer (Bremen, Germany). The liquid chromatograph was equipped with a KINETEX® XB-C18 column (2.1 mm×100 mm, 2.6 μm; Phenomenex). Mobile phase A consisted of 5% (v/v) acetonitrile in water and 0.1% (v/v) formic acid, whereas mobile phase B consisted of 95% (v/v) acetonitrile and 0.1% (v/v) formic acid. The gradient was 0–3 min (isocratic at 95% A), 3–35 min (increase to 100% B), 40–41 min (decrease to 95% A), and column equilibration for 9 min at initial conditions (95% A). The chromatographic run lasted 40 min with a flow rate of 0.2 ml min^{-1}. The mass spectrometer was operated in negative mode. The mass spectrometer's settings were: dry gas flow rate, 8 l min^{-1} at 220 °C; capillary voltage, 3.8 kV; collision energy, 10 eV; and collision radiofrequency, 1200 Vpp. The qTOF was operated with the *m/z* range set from 50 Da to 1500 Da. The injection volume was 10 μl. Acquisition of LC-MS data was performed using Bruker DataAnalysis 4.3.

Statistical analysis

Statistical analysis was performed with GenStat 17th Edition (a VSNI product: https://www.vsni.co.uk/software/genstat/). One-way ANOVA [Fisher's protected least significant difference (LSD) test $P<0.05$] was used to determine the statistical significances for the Chl data, RT-qPCR data, and nCounter data for a period of 72 h of dark treatment in WT L*er*-0. A linear mixed model was used to determine the differences for the data of 6 h and 18 h treatments in both WT and *max1-5/dis15* (with *rac*-GR24 or 1% DMSO treatment). Comparisons among means were made using LSDs at $P=0.05$ (5% LSD). CL and CLA data were analysed using one-way ANOVA. To equalize the variances, the variables were log transformed prior to analysis. Comparisons among means were made using 5% Fisher's LSDs.

Accession numbers

Gene and protein accession numbers are listed in Supplementary Table S5.

Results

Two EMS mutants exhibit delayed dark-induced senescence of excised immature inflorescences

We identified two EMS mutants with immature inflorescences that when detached and held in the dark exhibited delayed sepal degreening compared with the WT. They were designated *delayed inflorescence senescence* (*dis*) *9* and *dis15* (Fig. 1A). We confirmed that their immature inflorescences retained more Chl than the WT at day 3 of dark incubation (Fig. 1B). Transcripts of senescence markers *SAG12* (Grbic, 2003) and *ANAC092* (Balazadeh *et al.*, 2010) were not detected in the freshly harvested inflorescences, and their increased transcript abundance was suppressed in the two mutants compared with the WT at 72 h of dark incubation (Fig. 1C, D). This suggested that the delayed degreening of the mutants resulted from slower progression of senescence.

Both mutants backcrossed to the L*er*-0 WT segregated ~3:1 (WT:mutant) for their delayed degreening trait (Supplementary Table S6), indicating that a single locus was responsible for their *dis* phenotype. These two mutants were also shorter and had more flowering stalks compared with the WT (Supplementary Fig. S3), traits that co-segregated with their *dis* phenotype. This suggested that the two *DIS* loci control senescence of excised immature inflorescences in the dark and flowering stem elongation and branching *in planta*.

dis9 *and* dis15 *also exhibit delayed sepal degreening* in planta

We hypothesized that the *DIS* loci in both mutants would also control sepal degreening during plant development because genes that are key for regulating dark-induced leaf senescence
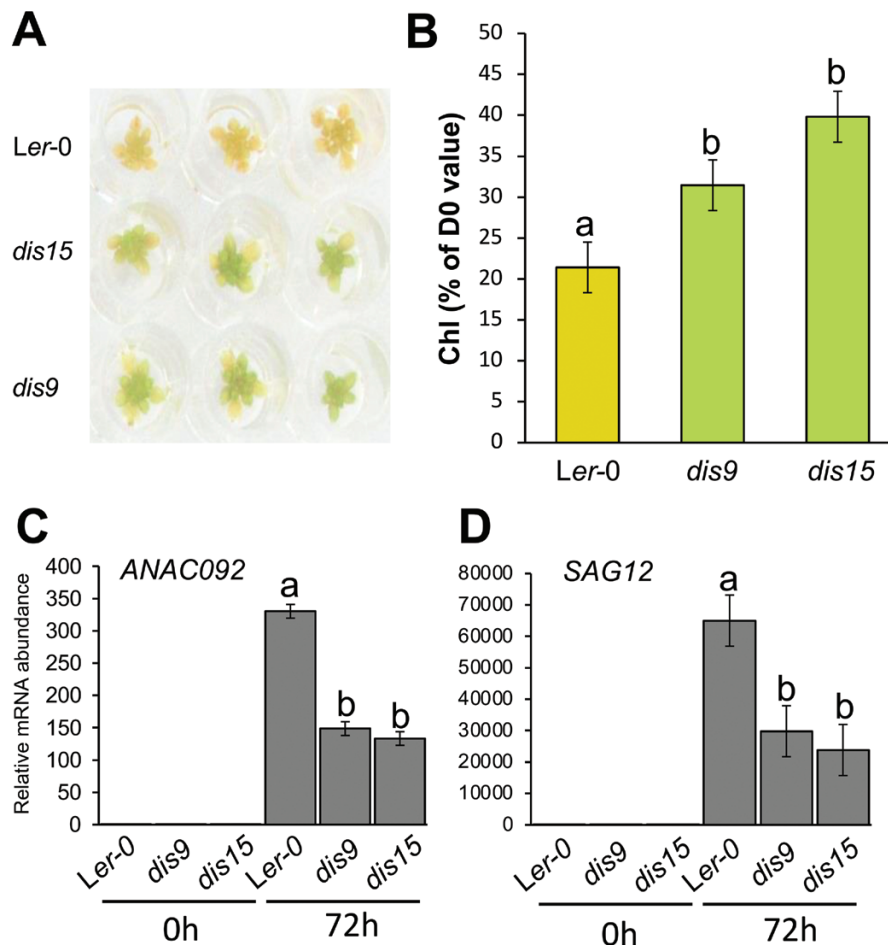

Fig. 1. Characterization of two EMS mutants displaying delayed degreening of excised dark-incubated inflorescences. (A) Degreening of dark-incubated inflorescences. Inflorescences were excised and placed in water and incubated in the dark for 5 d. Three biological replicates are shown. (B) Total chlorophyll retention (% of day 0 value) at day 3 of dark incubation. Data are means ±SE (*n*=6). Letters represent significant differences between L*er*-0 and *dis* mutants in one-way ANOVA (Fisher's protected LSD test *P*<0.05). (C) Transcript abundance of *ANAC092* in L*er*-0 and *dis* mutants at 0 and 72 h. (D) Transcript abundance of *SAG12* in L*er*-0 and *dis* mutants at 0 and 72 h. Transcript abundance was normalized to that of *PP2AA3* and expressed relative to L*er*-0 at 0 h. Data are means ±SE (*n*=3). Letters represent significant differences between L*er*-0 and *dis* mutants at 72 h dark incubation for each gene comparison in one-way ANOVA (Fisher's protected LSD test *P*<0.05). Means with the same letter denote not significantly different between *dis9* and *dis15*.

also regulate natural senescence (J. Kim *et al.*, 2018). We grew plants for 4–5 weeks in long-day conditions to allow the floral organs to develop and observed the colour of the sepals when they started to abscise. In four independent experiments, the sepals of the mutants were always green when they abscised, whereas in comparable WT plants they were yellow (Fig. 2A, B; Supplementary Fig. S4). The delayed sepal yellowing also occurred in the detached inflorescences that were incubated in long-day conditions (Fig. 2C; Supplementary Fig. S4). This indicated that in addition to affecting the timing of dark–induced degreening, the *DIS* loci also controlled sepal degreening *in planta* and in detached inflorescences held in long days.

dis9 *and* dis15 *have point mutations in* AtD14 *and* MAX1*, respectively*

Both mutants were crossed to Col-0 for mapping purposes, and their causal mutations were identified using a combination of high resolution melting (HRM)-based mapping and whole-genome sequencing analysis. The *dis9* mutation was identified as a C to T transition at position 290 downstream of the translation start site (TSS) of the Arabidopsis *D14* gene (*AtD14*, AT3G03990) (Supplementary Fig. S1A), encoding a α/β-fold hydrolase protein that functions as an SL receptor (Arite *et al.*, 2009; Yao *et al.*, 2016). The mutation causes a substitution of Ser to Phe at position 97 (S97F) of AtD14. The *dis15* mutation was identified as a G to A transition at position 1405 downstream of the TSS of the coding

sequence of the *MAX1* gene (AT2G26170) (Supplementary Fig. S1B). This mutation resulted in a substitution of Gly to Arg at position 469 (G469R) in the MAX1 cytochrome P450 monooxygenase (Booker *et al.*, 2005) that is involved in SL biosynthesis converting CL to CLA (Abe *et al.*, 2014). The *dis9* and *dis15* degreening phenotypes were complemented by WT *AtD14* and *MAX1* genomic regions, respectively (Supplementary Figs S5, S6). These two mutants were therefore renamed *d14-6/dis9* and *max1-5/dis15*, respectively.

Highly conserved amino acids are substituted in AtD14 and MAX1

The D14-S97F substitution in *d14-6/dis9* occurred in the Ser–His–Asp catalytic triad responsible for hydrolase activity of the receptor (Abe *et al.*, 2014). The importance of the Ser97 residue for hydrolase activity is supported by its high conservation in orthologues from other species (Arite *et al.*, 2009; Gao *et al.*, 2009; Liu *et al.*, 2009; Hamiaux *et al.*, 2012; de Saint Germain *et al.*, 2016; Zheng *et al.*, 2016) and the paralogue AtKAI2 (Waters *et al.*, 2012) (Fig. 3A). It is also supported by the finding that replacing Ser with a non-nucleophilic residue abolishes activity of the receptor protein expressed *in vitro* (Abe *et al.*, 2014) and prevents formation of a covalently linked intermediate molecule (CLIM) in the active site of the protein (Yao *et al.*, 2016) (Fig. 3B). Therefore, the SL-defective phenotype of *d14-6/dis9* strongly suggested that substitution
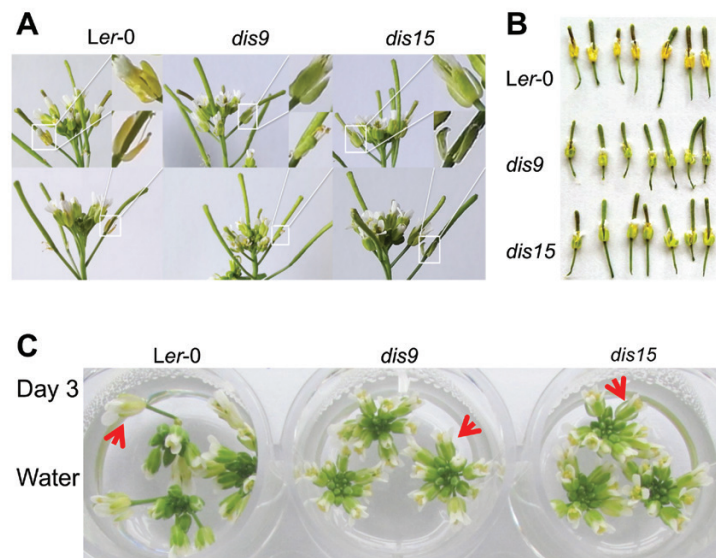

Fig. 2. Delayed sepal degreening of *dis9* and *dis15 in planta* and in detached immature inflorescences held in long-day conditions. (A) Inflorescences attached to plants. Inflorescences from the primary bolts of 4.5-week-old wild-type and *dis* plants were photographed. Two biological replicates with representative abscising sepals (in white squares and magnified) are shown. (B) Degreening of sepals *in planta*. Flowers of 5-week-old plants were harvested when their sepals were just starting to abscise. Each flower of the seven biological replicates is from an independent plant. (C) Sepal degreening of excised inflorescences. Inflorescences were harvested from the primary bolts of 4.5-week-old plants that had their first flower opened on the same day. The inflorescences with removed opened buds were placed in water and incubated for 3 d. Three biological replicates are shown. Representative sepals are indicated by red arrows.

of Ser97 to Phe (a non–nucleophilic amino acid) also caused loss of receptor activity *in planta*.

The *MAX1*-G469R substitution in *max1-5/dis15* occurred in the last residue of the Cys haem–iron ligand signature [FW]-[SGNH]-x-[GD]-{F}-[RKHPT]-{P}-C-[LIVMFAP]-[GAD], which is highly conserved in the cytochrome P450 superfamily (Prosite: https://prosite.expasy.org/PDOC00081).

This G469 residue is invariant in all MAX1 functional orthologues studied thus far (Fig. 3C) (Yoneyama *et al.*, 2018). However, as the ligand signature [GAD] indicates, Gly (G) can be replaced by Ala (A) or Asp (D). This occurs at very low frequency in the wider cytochrome P450 protein family, with G replaced by A in 3.4% or by D in 0.18% of the 1087 predicted cytochrome P450 proteins that have the Cys haem–iron ligand
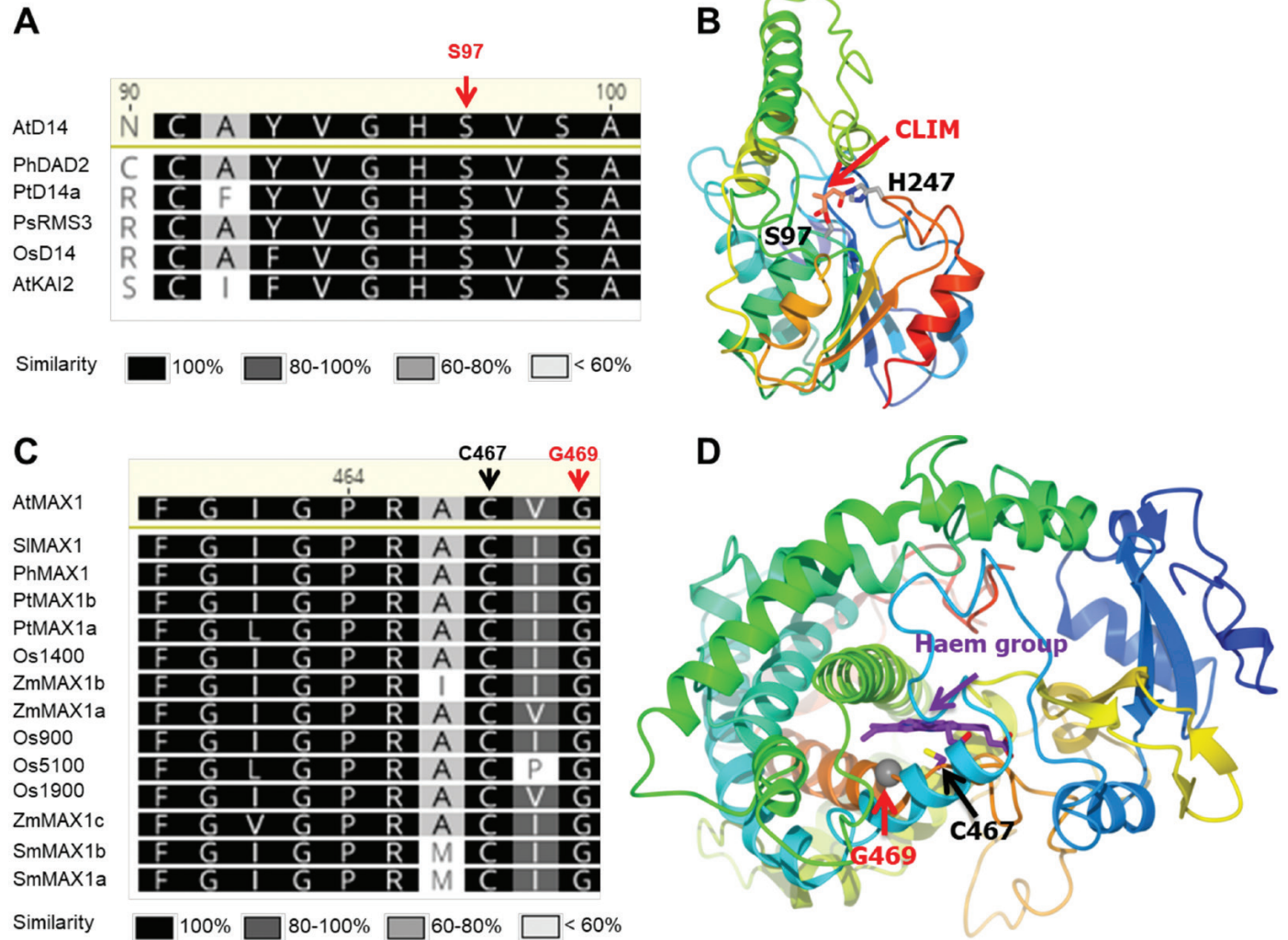

Fig. 3. Location of the substituted amino acids in the D14 and MAX1 proteins. (A) Sequence alignment of Arabidopsis D14 with characterized homologues. The position of the mutation at Ser97 (S97) in AtD14 is indicated in red. Amino acid positions are based on the Col-0 sequence from TAIR. Aligned sequences were sorted by the differences from the AtD14 reference sequence. Intensity of shading represents the percentage similarity of each residue among characterized D14 orthologues. At, Arabidopsis; Os, rice; Ph, petunia; Pt, poplar; Ps, pea; and the paralogue AtKAI2. (B) Structure of AtD14 from the SL-induced AtD14–D3–ASK1 complex (PDB: 5HZG). The covalently linked intermediate molecule (CLIM) is shown as orange and red sticks. The catalytic triad residues Ser97 and His247 are shown in atomic colouring as grey/blue/red sticks. AtD14 is shown in cartoon representation coloured in a rainbow scheme (N- to C- terminus from blue to red). (C) Sequence alignment of Arabidopsis MAX1 with its functional orthologues showing the cysteine haem–iron ligand signature. The position of the mutation at Gly469 (G469) and of the haem–iron ligand at Cys467 (C467) in Arabidopsis MAX1 is indicated in red and black, respectively. Amino acid positions are based on the Col-0 sequence from TAIR. Aligned sequences were sorted by the differences from the AtMAX1 reference sequence. Intensity of shading represents the percentage similarity of each residue among MAX1 orthologues. At, Arabidopsis; Sl, tomato; Sm, *Selaginella*; Os, rice; Ph, petunia; Pt, poplar; Zm, maize. (D) MAX1 modelled on the structure of the closely related human cytochrome P450 CYP3A4 (PDB: 1TQN). The haem group is presented as purple sticks (carbons mostly), which is indicated by a purple arrow. The side chain of Cys467 (in black; haem ligand) is represented by sticks (carbon is purple and sulfur is yellow). The position of Gly469 is indicated by the grey sphere and is highlighted by a red arrow. The structure is presented in cartoon representation coloured in a rainbow scheme (N- to C- terminus from blue to red).

pattern (according to the Prosite database) (Supplementary Fig. S7). We modelled the 3D structure of AtMAX1 on the most closely related cytochrome P450 (human cytochrome P450 CYP3A4) (Yano *et al.*, 2004) with a protein crystal structure available (sequence identity of 28% and E-value of 7e-51). The model showed that G469 is in the haem pocket, packed against the haem group and close to the haem–iron ligand Cys (Cys467) (Fig. 3D).

G469R substitution in max1-5/dis15 *disrupts enzyme activity of MAX1*

To confirm the loss of activity of *MAX1*-G469R suggested by *in silico* prediction, we used transient expression in *N. benthamiana*, as developed to study the function of SL biosynthetic enzymes (Zhang *et al.*, 2014). Arabidopsis *MAX1*-WT, *MAX1*-G469R, and *MAX1*-G469A were transiently expressed with the upstream enzyme-encoding genes of the CL biosynthetic pathway (*AtD27*, *AtMAX3*, and *AtMAX4*), then the substrate (CL) and product (CLA) of MAX1 were measured. As expected, transient expression of *AtD27*, *AtMAX3*, and *AtMAX4* resulted in the production of CL and not CLA (Fig. 4A). When co-expressed with *MAX1*-WT (either the L*er*-0 or Col-0 version) or *MAX1*-G469A, CL was significantly reduced and some CLA was detected. However, when co-expressed with *MAX1*-G469R, the amount of CL did not

decrease although CLA was produced in similar amounts to that produced by *MAX1*-WT (Fig. 4A). The lack of a decrease in CL suggested that *MAX1*-G469R had reduced enzymatic activity. We considered that the absence of a difference in CLA production in the different treatments was likely to be caused by conjugation (e.g. glycosylation) of CLA by endogenous *N. benthamiana* enzymes, since we had observed this several times previously in *N. benthamiana* (e.g. in the transient production of geranic acid that was glycosylated with one or two hexoses; Dong *et al.*, 2013). If CLA conjugation occurs efficiently, the amounts of free CLA would remain low and not reflect the rate of conversion of CL to CLA. Thus, we investigated whether *N. benthamiana* leaves expressing *MAX1*-WT accumulated CLA conjugates using LC-qTOF-MS analysis. Indeed, *N. benthamiana* leaves expressing the CL pathway genes together with *MAX1*-WT accumulated CLA–dihexose and CLA–hexose conjugates (Fig. 4B; Supplementary Fig. S8). When *MAX1*-G469A was substituted for *MAX1*-WT, conjugate formation was not significantly different from that in the pathway with *MAX1*-WT (Fig. 4B; Supplementary Fig. S8). However, when *MAX1*-G469R was substituted for *MAX1*-WT, conjugate production decreased 36- and 15-fold, respectively. To confirm that the G469R mutation was affecting enzyme activity rather than exerting its effect through transcriptional changes, mRNA abundance of *MAX1*-WT and *MAX1*-G469R was analysed. There was no difference in
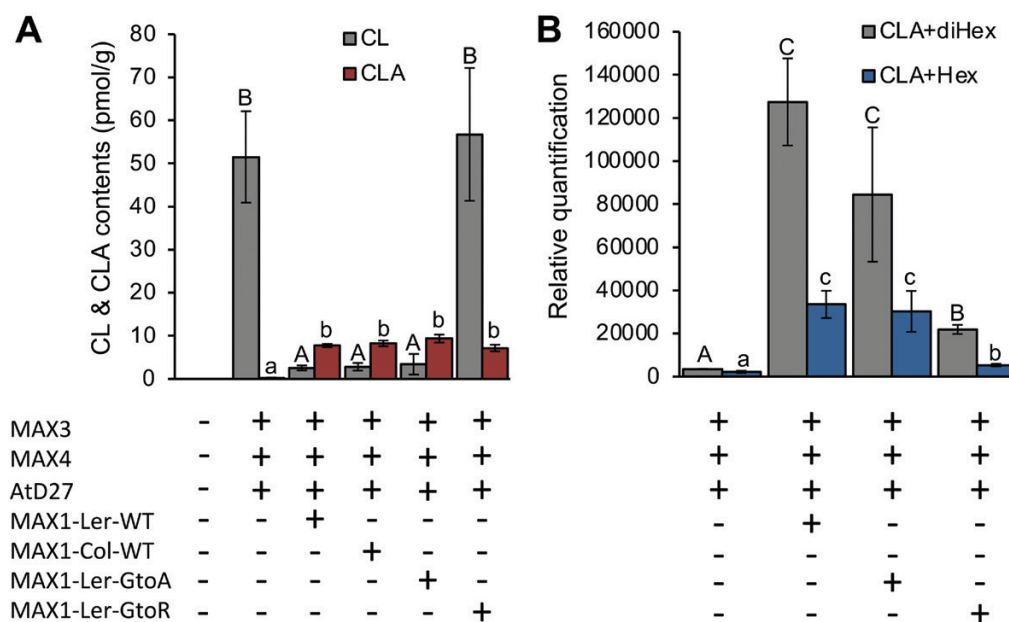

Fig. 4. Analysis of CL, CLA, and CLA conjugates in *N. benthamiana* leaves infiltrated with strigolactone biosynthetic gene constructs. (A) CL and CLA content in *N. benthamiana* transiently expressing *MAX1* (Col/L*er*-WT or with nucleotide changes resulting in G469R or G469A substitutions) plus three CL pathway genes (*AtD27*, *AtMAX3*, and *AtMAX4*). Data are the mean ±SE (*n*=6). (B) Identification of CLA conjugates in *N. benthamiana* transiently expressing *MAX1*-L*er*/G469R/G469A plus CL pathway genes. Data are the mean ±SE (*n*=3). Relative quantification based on mass intensity. EV, empty vector (control). Letters represent significant differences among different gene combinations for the infiltration for each compound comparison in one-way ANOVA. Upper and lower case were used to distinguish the difference for each compound in (A) and (B). Means for the same compound with the same letter are not significantly different (5% least significant difference comparisons made on log-transformed data).

expression between *MAX1*-WT and *MAX1*-G469R when they were expressed in *N. benthamiana* (Supplementary Fig. S9). Thus, we concluded that the lack of CL conversion and reduced CLA conjugate production in *N. benthamiana* upon co-infiltration of the CL pathway with *MAX1*-G469R was caused by reduced activity of the MAX1-G469R enzyme.

SL biosynthetic and response genes are up-regulated by 24 h of dark incubation in inflorescences

The SL biosynthetic pathway is thought to be induced by senescence signalling (Ueda and Kusaba, 2015). To test this, we used nCounter technology to compare the timing of transcriptional changes in selected senescence marker and SL pathway genes in excised WT inflorescences every 24 h over a period of 3 d of dark treatment.

The transcript abundance of early stage senescence markers, namely *ANAC092* and the Chl degradation gene *SGR1* (Park *et al.*, 2007), significantly increased at 24 h (Fig. 5A), suggesting senescence in the inflorescences had already initiated by this time. Increased transcript abundance of the late stage senescence-specific marker gene *SAG12* at 48 h indicated that at 2 d of dark incubation senescence was well advanced.

The transcript abundance changes of three SL biosynthetic genes, *MAX1*, *MAX3*, and *MAX4*, was used to estimate when SL biosynthesis was initiating in the dark-held inflorescences. *MAX1* transcript abundance did not significantly change during the first 24 h of dark treatment, but then significantly and substantially increased to be highest at 72 h (Fig. 5B). *MAX3* transcript abundance was slightly increased at 24 h, suggesting that SL production in the tissue was just starting. From 24 h onwards, *MAX3* transcript abundance increased in concert with both early senescence markers *SGR1* and *ANAC092*. RT-qPCR analysis of *MAX4* revealed a pattern of transcript accumulation that was very similar to that of *MAX3*, suggesting co-regulation and the beginning of SL synthesis by 24 h (Supplementary Fig. S10A).

We examined changes in the transcript abundance of the SL signalling genes *AtD14*, *SMXL6*, *SMXL7*, and *SMXL8*. Transcript abundance of the first three genes increased significantly at 24 h of dark treatment (Fig. 5C, D), whereas *SMXL8* transcript abundance decreased to be undetectable at 24 h (Fig. 5D). The nCounter results for *MAX3*, *SMXL6/8*, *ANAC092*, and *SAG12* were confirmed by RT-qPCR analysis (Supplementary Fig. S10). Overall, the results from the transcript profiling of the inflorescence suggested that, by 24 h of dark incubation, SL biosynthesis has been initiated, SL signalling is occurring, and senescence has started. Thus, earlier time points were investigated to determine the order of pathway activation.

SL signalling, but not biosynthetic, genes respond rapidly to the light–dark transition

At 24 h of darkness, the inflorescence tissue had been exposed to 8 h of regular and 16 h of extended night. Holding tissue

in extended darkness leads to acute carbon starvation caused by exhaustion of starch reserves (Usadel *et al.*, 2008) that can lead to precocious senescence. To test whether SL biosynthesis and response were associated with carbon deprivation–based signalling, we compared the timing of expression of transcriptional markers of tissue carbon status (SnRK1-related genes *AKINβ1* and *bZIP63*) (Bläsing *et al.*, 2005; Usadel *et al.*, 2008; Li *et al.*, 2009; Mair *et al.*, 2015) with that of SL-associated genes in both the regular and the early extended night.

In L*er*-0 controls during the first 6 h into the regular night, transcript abundance of *AKINβ1* and *bZIP63* increased in the detached WT inflorescences held in the dark (Fig. 6A) consistent with the genes being markers of reduced carbohydrate status. Key senescence-regulatory genes *ANAC092* (Kim *et al.*, 2009) and *AtNAP* (Guo and Gan, 2006) were up-regulated at 3 h (Fig. 6B) probably because of their known induction by reduced sugar status (Bläsing *et al.*, 2005; Usadel *et al.*, 2008) and/or the circadian clock (H. Kim *et al.*, 2018; Song *et al.*, 2018). There was no increase in transcript abundance of *MAX1* 6 h into the regular night, and *MAX3* transcripts were not detected at this time (Fig. 6C). Transcript abundance of *SMXL7* also did not change during the regular night (Fig. 6D). However, at 3 h into the dark period, *SMXL6* and *SMXL8* were up- and down-regulated, respectively (Fig. 6D).

In order to determine the effect of SL on the expression of the above genes, we treated the inflorescences with *rac*-GR24. *Rac*-GR24 is a racemic mixture of two enantiomers, GR24^5DS a synthetic canonical SL, and GR24^ent-5DS that induces karrikin (KAR) signalling (Kramna *et al.*, 2019). However, GR24^ent-5DS is probably not relevant for the dark-induced degreening phenotype since defects in KARRIKIN INSENSITIVE 2 (KAI2), a KAR-specific receptor, do not delay dark-induced leaf senescence (Ueda and Kusaba, 2015). In the mock-treated *max1-5/dis15* mutant, the two *MAX* and three *SMXL* genes exhibited similar expression patterns to that of the WT, although their abundance was lower (Fig. 6C, D). The reduced expression of the three *SMXL* genes was reversed when the mutant was treated with 5 μM *rac*-GR24 for 3 h (Fig. 6D). Intriguingly, *AtNAP* was up-regulated by *rac*-GR24 at 3 h of treatment (Fig. 6B), suggesting that it is also an SL-inducible gene. Thus, based on transcription, the increased transcript abundance of sugar-related genes did not induce expression of SL biosynthetic genes in the WT inflorescences during the normal night. In the *max1-5/dis15* mutant, both SL signalling genes and *AtNAP* respond rapidly to *rac*-GR24 treatment, indicating that these genes were SL inducible.

GR24 induces the transcript abundance of senescence-related genes in max1-5/dis15 during an extended night

We next determined the effect of extended darkness (i.e. darkness that surpassed the anticipated night period) on
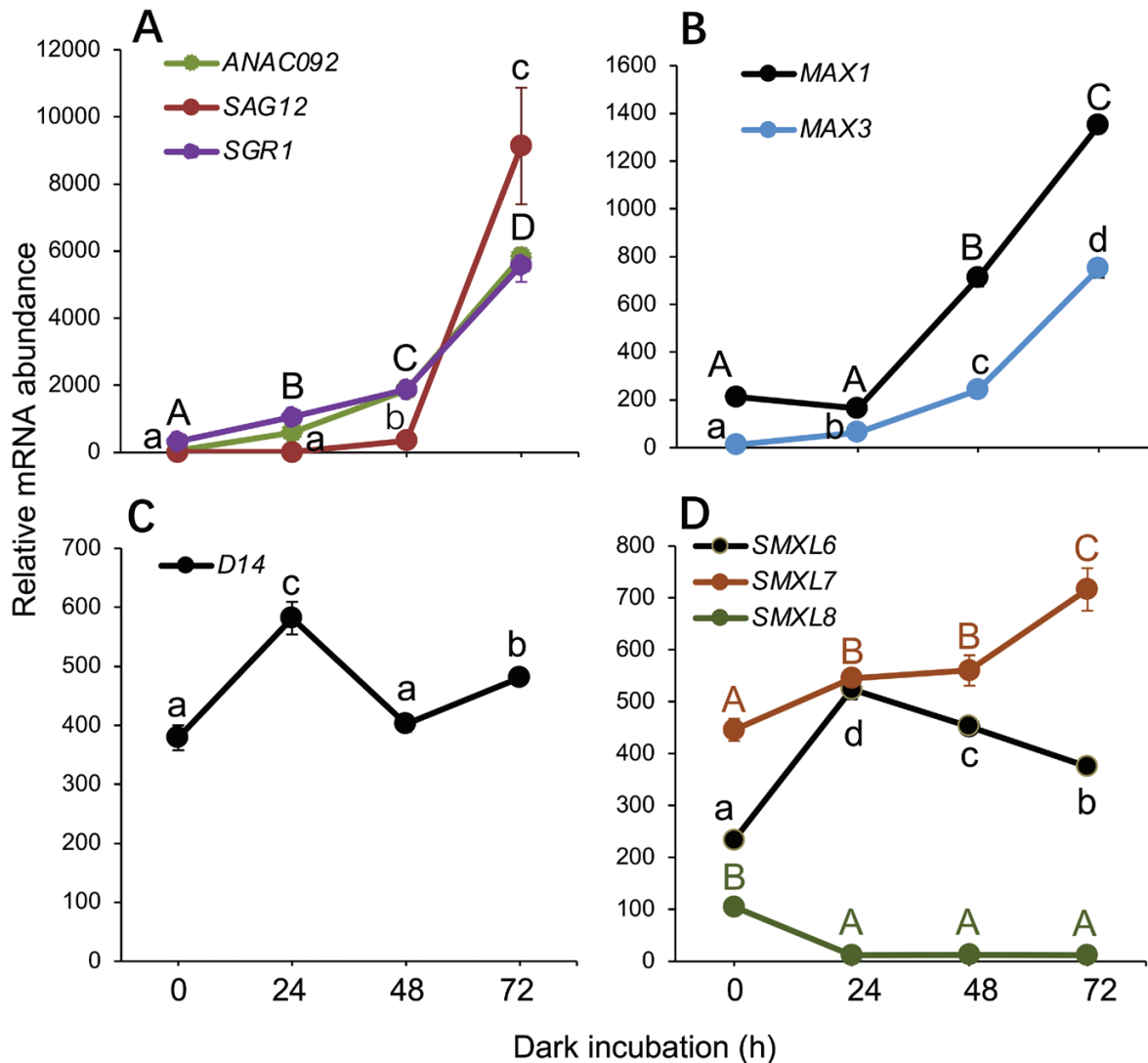
Fig. 5. Dark-induced transcript abundance changes of strigolactone pathway and senescence-related genes. (A) Chlorophyll (Chl) degradation and senescence marker genes. (B) SL biosynthetic genes. (C) SL receptor. (D) SL signalling genes. Transcript abundance was quantified using nCounter technology on RNA isolated from detached WT inflorescences (*n*=3 samples, >4 inflorescences from independent plants per sample) that were incubated in the dark for 0, 24, 48, and 72 h. Transcript abundance was normalized to the geometric mean of *PP2AA3*, *ACT2*, and *MON1*. Data are the mean ±SE. Letters represent significant differences among four time points for each gene comparison in one-way ANOVA (Fisher's protected LSD test *P*<0.05). Upper and lower case letters were used to distinguish the comparisons for each gene. Upper case letters in (A) represented comparisons for both *ANAC092* and *SGR1*.

carbon status markers, senescence markers, and SL biosyn-thesis and signalling genes. In the WT, at 4 h of extended night (i.e. 12 h of dark treatment), transcript abundance of *AKINβ1* and *bZIP63* was substantially increased (Fig. 7A). This was consistent with the WT inflorescences experiencing carbon starvation, as has been reported for rosette leaves ex-posed to a 4 h extended night (Usadel *et al.*, 2008). Transcript abundance of *ANAC092* and *AtNAP* was also significantly increased at this time (Fig. 7B). However, in L*er* controls, transcript abundance of *MAX1* was not increased by the 4 h night extension, and *MAX3* abundance remained undetect-able, suggesting that SL biosynthesis was still not occurring. By 10 h of extended night (18 h of dark treatment), *MAX1*

transcript abundance had still not changed, but that of *MAX3* had increased, suggesting that SL biosynthesis had started (Fig. 7C). The three *SMXL* genes were differentially ex-pressed during the extended night (Fig. 7D). *SMXL8* tran-script counts were almost undetectable at both 12 h and 18 h; *SMXL6* transcript abundance was increased at 12 h but then declined; and *SMXL7* started to increase at 18 h in a pattern similar to *MAX3*.

We then determined how the patterns of expression of the above genes were affected by SL deficiency by examining their transcript accumulation in the *max1-5/dis15* mutant. Overall, in the mock-treated *max1-5/dis15* mutant, the patterns of ac-cumulation of carbon status–related genes, senescence marker
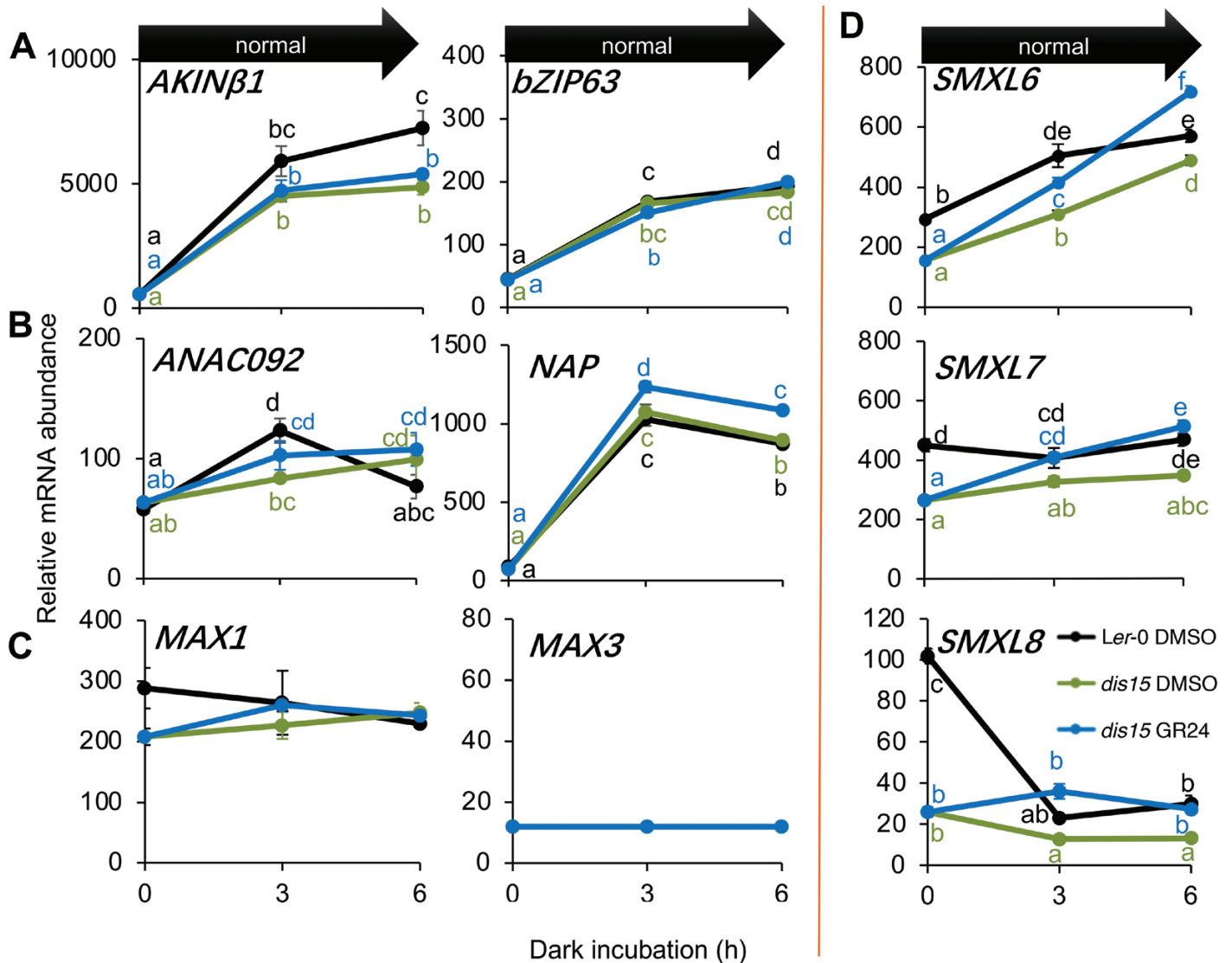
Fig. 6. Transcript abundance of strigolactone pathway genes during regular night. (A) SnRK1-related genes. (B) Functional senescence regulators. (C) SL biosynthetic genes. (D) SL signalling genes. Transcript abundance was quantified using nCounter analysis on RNA isolated from detached WT or *max1-5/dis15* inflorescences (*n*=3 samples, >4 inflorescences from independent plants per sample) that were treated with 1% DMSO or 1% DMSO containing 5 μM *rac*-GR24 as indicated, then incubated in the dark for 0, 3, and 6 h. Transcript abundance was normalized to the geometric mean of *PP2AA3*, *ACT2*, and *MON1*. Data are the mean ±SE. Different letters indicate statistical difference (*P*=0.05).

genes, and SL biosynthesis and signalling genes in the mutant were very similar to that seen in the WT over the 10 h extended night (Fig. 7), suggesting that their pattern of regulation was not controlled by SL. Interestingly, when the mutant was treated with *rac*-GR24, the transcript abundance of sugar-related genes *AKINβ1* and *bZIP63* was suppressed significantly at 12 h but not at 18 h (Fig. 7A). In contrast, the transcript abundance of the two senescence-related genes *ANAC092* and *AtNAP* was elevated at 12 h (4 h of extended night) by *rac*-GR24, and so was *MAX1* (Fig. 7B, C). All three *SMXL* genes were up-regulated by *rac*-GR24 at both time points (Fig. 7D), as observed during the regular night.

Taken together, the nCounter profiling study has highlighted a temporal sequence of events whereby markers of

carbon deprivation and senescence regulation first increased, followed within hours by markers for SL production. Further, GR24 treatment of the *max1-5/dis15* mutant indicated that SL acts to promote transcription of senescence-controlling genes and to suppress transcription of SnRK1-related genes.

Discussion

Mutations in SL biosynthesis and receptor proteins define functionally important amino acids

The finding with an EMS screen of two independent mutations in the SL pathway that significantly affected sepal senescence progression emphasizes the importance of this hormone
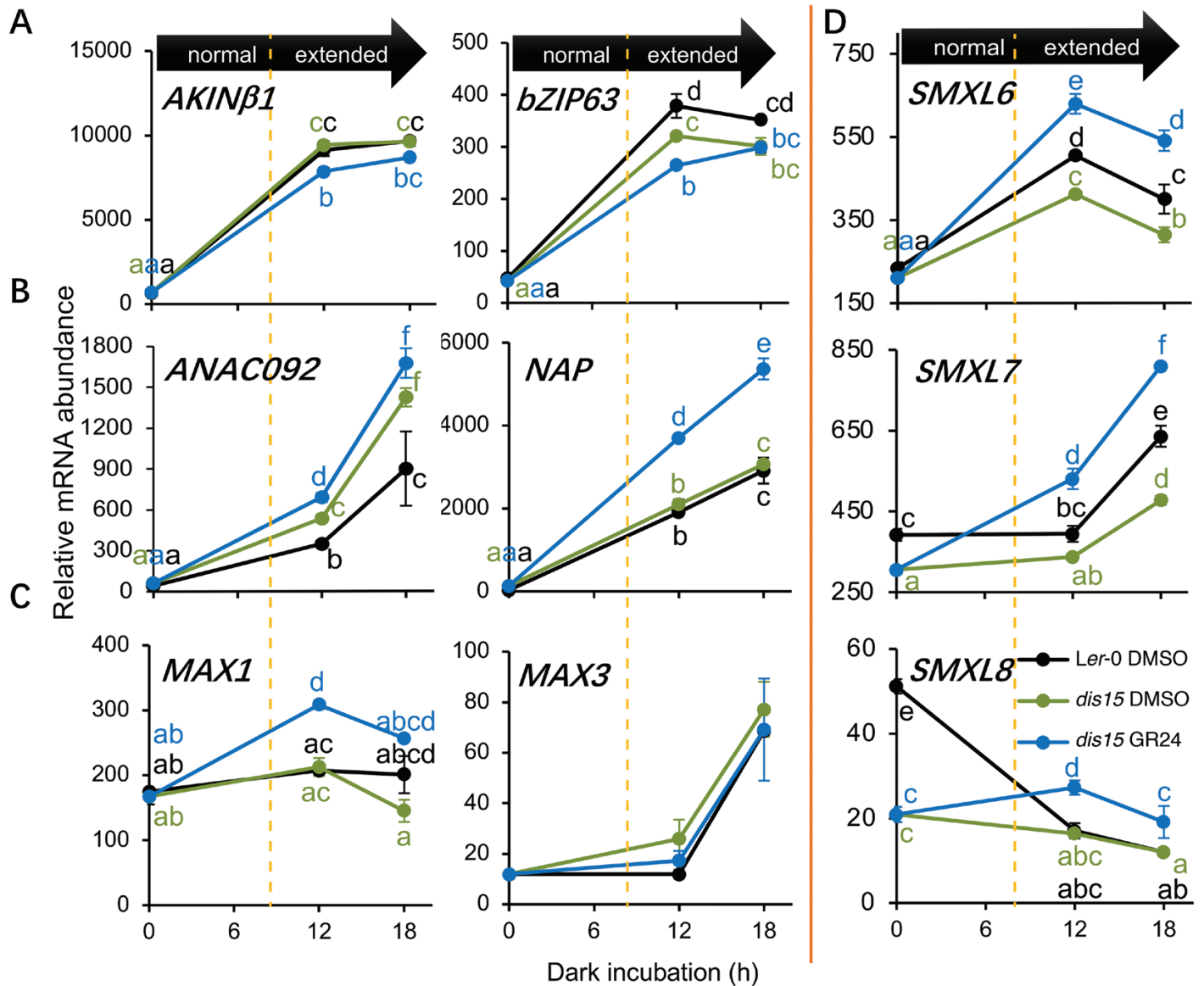
Fig. 7. Transcript abundance of sugar, senescence, and strigolactone pathway genes during an extended night. (A) SnRK1-related genes. (B) Functional senescence regulators. (C) SL biosynthetic genes. (D) SL signalling genes. Transcript abundance of each gene was quantified using nCounter technology on RNA isolated from detached WT or *max1-5/dis15* inflorescences (*n*=3 samples, >4 inflorescences from independent plants per sample) that were treated with 1% DMSO or 1% DMSO containing 5 µM *rac*-GR24 as indicated, and incubated in the dark for 0, 12, and 18 h. The normal night is considered as 8 h. Transcript abundance was normalized to the geometric mean of *PP2AA3*, *ACT2*, and *MON1*. Data are the mean ±SE.

in the floral death process in addition to its more explored roles in plant development (Gomez-Roldan *et al.*, 2008; Umehara *et al.*, 2008; Kapulnik *et al.*, 2011; Ruyter-Spira *et al.*, 2011; Rasmussen *et al.*, 2012; Toh *et al.*, 2012).

MAX1 encodes a CYP711A1 protein of the cytochrome P450 superfamily (Booker *et al.*, 2005). The *MAX1*-G469R substitution occurred at the last residue in the highly conserved Cys haem–iron ligand signature, which is just two amino acids C-terminal to the absolutely conserved Cys at position 467. To date, no crystal structure of MAX1 has been reported. However, a 3D model based on the closest homologous structure, the

human microsomal P450 CYP3A4, revealed that Gly469 packs against the haem cofactor in the binding pocket and is close to the haem–iron ligand Cys467 (Fig. 3D). The G469R substitution presumably causes loss of function by disrupting the steric structure of this pocket because there is not enough space to accommodate Arg, which has one of the largest side chains, compared with Gly that has the smallest.

The G469 residue is invariant in MAX1 orthologues and its closely related proteins in Metazoa, Bacteria, and Archaea (Fig. 3C; Supplementary Fig. S7; Challis *et al.*, 2013), whereas in the wider cytochrome P450 family in rare instances this

residue is replaced by Ala. Our transient expression assay in *N. benthamiana*, and successful genetic complementation of the *max1-5/dis15* mutant with *MAX1*-G469A (Supplementary Fig. S6) demonstrated that the Ala substitution did not reduce MAX1 function, suggesting that this small non-polar amino acid does not introduce steric clashes in the wider family of cytochrome P450 proteins either. This is consistent with the equivalent Gly to Ala substitution not affecting activity of the Arabidopsis cytochrome P450 CYP83B1, a modulator of auxin homeostasis (Barlier *et al.*, 2000; Bak *et al.*, 2001). The high content of CL and strongly reduced production of CLA hexose conjugates in the leaves infiltrated with the *MAX1*-G469R construct are consistent with accumulation of CL previously observed for the Arabidopsis T-DNA insertion mutant *max1-4* (Seto *et al.*, 2014), which indicates that conversion of the MAX1 substrate is inhibited. Thus, G469 is an important amino acid for MAX1 function, though it can be replaced by Ala.

The crystal structures of AtD14 and its orthologues in petunia (PhDAD2) and rice (OsD14) show that they have a hydrophobic substrate-binding pocket containing a Ser–His–Asp catalytic triad essential for hydrolase activity (Hamiaux *et al.*, 2012; Kagiyama *et al.*, 2013; Zhao *et al.*, 2013). Unlike the classical hormone receptors that non-covalently and reversibly bind to hormone molecules, the crystal structure of the SL-induced AtD14–D3–ASK1 complex reveals that AtD14 binds to SL and hydrolyses it into a CLIM (Yao *et al.*, 2016). It is under debate whether this hydrolysis is required for signalling to occur (Seto *et al.*, 2019). Experiments with the F-box protein D3, a rice orthologue of Arabidopsis MAX2, showed that SL triggers signalling by enabling AtD14 to bind to MAX2 to recruit repressors (e.g. Arabidopsis SMXL6/7/8) for degradation through the 26S proteasome (Jiang *et al.*, 2013; Zhou *et al.*, 2013; Wang *et al.*, 2015). In the *d14-6/dis9* mutant, Ser97 in the catalytic triad was replaced by Phe. This produced phenotypes similar to the null mutant *d14-1*, suggesting loss of activity of D14 (Waters *et al.*, 2012; Ueda and Kusaba, 2015). It is also consistent with mutation of this residue to another non-nucleophilic residue, Ala (atd14:S97A), abolishing hydrolase activity *in vitro* of the expressed protein (Abe *et al.*, 2014). Thus, it is probable that the *in planta* S97F mutation we identified causes complete loss of D14 activity by affecting its hydrolase activity.

SLs regulate dark-induced inflorescence senescence in association with a change of carbon status during extended night

Our results indicated that SLs hastened Arabidopsis sepal senescence *in planta* and under energy deprivation conditions. Previously we showed that dark treatment of detached inflorescences was associated with reduced soluble sugar content and transcriptional changes of sugar-related genes (Trivellini *et al.*, 2012). Thus, it was plausible that SLs would interact with sugar

signalling to control dark-induced inflorescence senescence, which would be consistent with reports of crosstalk between SLs and sugar regulation of shoot branching and seedling establishment in Arabidopsis (Li *et al.*, 2016; Otori *et al.*, 2017), and the finding that SL-induced senescence of bamboo leaves is suppressed by exogenous sugar treatment (Tian *et al.*, 2018).

SL and sugar interaction during normal night

In the inflorescences, genes that control sugar-dependent transcriptional response (Bläsing *et al.*, 2005; Baena-González *et al.*, 2007; Usadel *et al.*, 2008), namely the SnRK1-related genes *AKINβ1* (a subunit of SnRK1) (Li *et al.*, 2009) and *bZIP63* (one of the direct targets of SnRK1) (Mair *et al.*, 2015), were up-regulated during the regular night, consistent with sugar status reducing as the night progressed. To determine whether this normal diurnal reduction in sugar content was associated with changes in SL content, we used the approach of Li *et al.* (2018) and measured transcript abundance changes of the SL biosynthetic genes because of the difficulty in measuring SLs in Arabidopsis (Seto *et al.*, 2014; Lv *et al.*, 2018), although we acknowledge that the involvement of post-transcriptional factors cannot be discounted. SLs did not appear to be synthesized in response to the sugar decline, since *MAX1* abundance was unchanged and *MAX3* counts were below the threshold for detection (Fig. 6A).

Mashiguchi *et al.* (2009) and Brewer *et al.* (2016) had suggested that such an interpretation could be confounded by SL negative feedback on SL biosynthetic genes. However, we did not find evidence for SL negative feedback since: (i) transcript abundance of the SL biosynthetic genes was not higher in the *max1-5/dis15* mutant and L*er*-0 WT; and (ii) treatment of the inflorescences with the SL analogue did not suppress their expression. This absence of negative feedback agrees with the findings of Bainbridge *et al.* (2005) on *MAX4*.

SL and sugar interaction during extended night

The extended night commences when the regular night ends. In Arabidopsis rosettes, a 4 h extended night leads to acute carbon deprivation and transcriptional reprogramming by SnRK1s (Baena-González *et al.*, 2007; Usadel *et al.*, 2008). Consistent with this, we found that *AKINββ1* and *bZIP63* transcripts increased to their highest abundance in both the WT and *max1-5/dis15* at 12 h (4 h into extended night) (Fig. 7). Transcripts of the senescence-regulating genes *ANAC092* and *NAP* continued to increase at 18 h and this corresponded to the time when *MAX3* and *SMXL7* started to increase. We used *SMXL6*, *SMXL7*, and *SMXL8* to determine SL response because the delayed senescence phenotype in both mutants was tightly linked to altered branching and these *SMXL* genes are functionally redundant in controlling Arabidopsis shoot branching (Soundappan *et al.*, 2015; Wang *et al.*, 2015). The expression pattern of *SMXL7* correlated best with the SL biosynthetic genes and senescence marker genes.
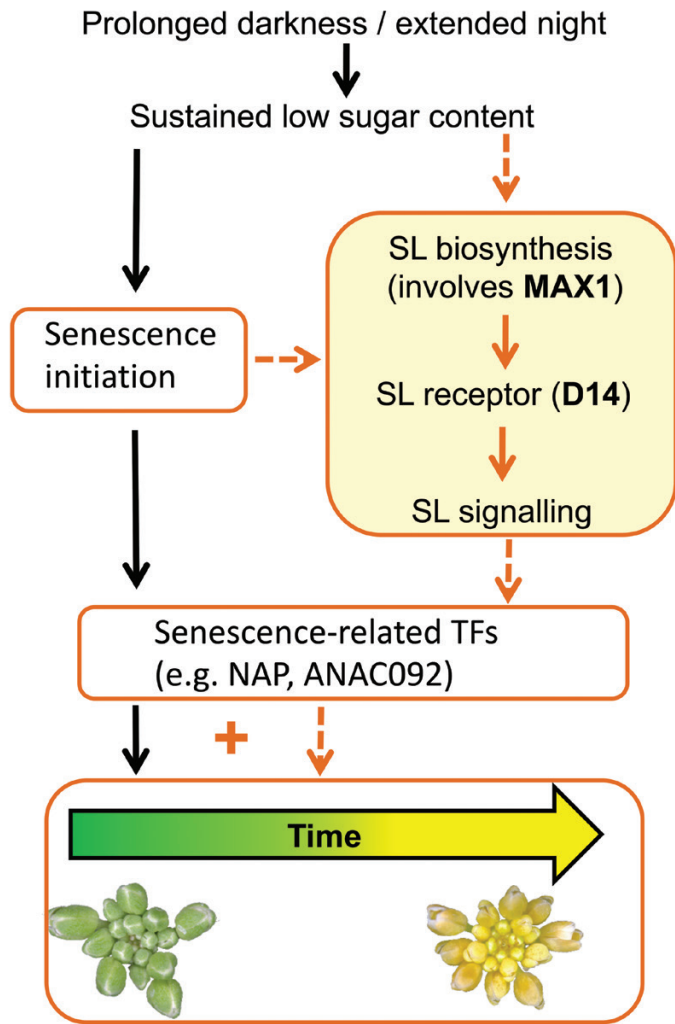
Fig. 8. Model for dark- and starvation-induced, SL-accelerated inflorescence senescence. Prolonged darkness causes sugar shortage, triggering senescence initiation and subsequent progression in detached inflorescences. This is accompanied by transcriptional changes of senescence-related transcription factor genes (TFs) such as *ANAC092* and *NAP*. The sustained low sugar content and consequent senescence initiation stimulates biosynthesis of SLs that then act to accelerate the progression of senescence by further activating key senescence regulators. Solid and dashed arrows indicate the characterized and speculated regulatory pathways, respectively. The SL pathway is shown in a yellow box. *MAX1* and *D14* in which the causal mutations were identified are highlighted in bold. The plus symbol highlights the enhancement of senescence rate by the presence of the SL pathway.

SMXL7 also has higher transcript abundance than *SMXL6* and *SMXL8* in senescent leaves (Stanga *et al.*, 2013), which suggests that this SMXL may have a more important role in senescence than the others.

In summary, two novel mutants have highlighted a connection between the SL pathway and floral organ senescence *in planta*, and in response to carbon limiting conditions. Our analyses indicated an intricate relationship among sugar starvation, senescence, and SL biosynthesis and signalling in excised dark-held inflorescences. Here we propose a model (Fig. 8) in which sugar shortage resulting from prolonged darkness triggers senescence initiation and progression in the inflorescence, and this associates with transcriptional changes of senescence-related transcription factor genes such as *NAP* and *ANAC092* (Trivellini *et al.*, 2012). SLs may not have a major role in the inflorescence during the normal night but are synthesized during the extended night, perhaps in response to sustained low sugar content and consequent senescence initiation. Then SLs play an important role in promoting senescence progression, perhaps by activation of key senescence regulators.

Supplementary data

The following supplementary data are available at JXB online.

Fig. S1. Identification of causal mutations in *dis9* and *dis15* mutants.

Fig. S2. Stability of PP2A reference gene expression in response to GR24 treatment and in a strigolactone-deficient mutant.

Fig. S3. The dwarf and bushy phenotypes of *dis9* and *dis15 in planta*.

Fig. S4. Delayed sepal degreening of *dis9* and *dis15 in planta* and in detached inflorescences held in long-day conditions.

Fig. S5. Genetic complementation of *dis9*.

Fig. S6. Complementation of *dis15* with *MAX1*-WT and *MAX1*-G469A.

Fig. S7. Sequence alignment of Arabidopsis MAX1 with its putative orthologues, related proteins, and other cytochrome P450 proteins with the haem–iron ligand signature.

Fig. S8. Identification of CLA conjugates in *N. benthamiana* leaves infiltrated with different combinations of SL biosynthetic genes.

Fig. S9. Transcript abundance of *MAX1* in leaves of *N. benthamiana* infiltrated with constructs harbouring *MAX1*-WT, -G469R, or -G469A.

Fig. S10. Transcript abundance changes of SL pathway and senescence–related genes.

Table S1. HRM primers for fine mapping of *dis9*.

Table S2. Primers for RT-qPCR analysis.

Table S3. Probes for nCounter analysis.

Table S4. Primers for MAX1-related constructs used in agroinfiltration of *N. benthamiana*.

Table S5. Gene and protein accession numbers.

Table S6. Pearson's χ^2 test for F_2 progenies of *dis9* and *dis15*.

Author contributions

XX, DAH, and PPD: conceptualization and design; XX, RJ, and AE: mutant screening; HB: overseeing transient expression, LC-MS, and qTOF analysis; XX, YW, LD, and KF: data analysis; XX and ARGM: statistics; XX and AH: nCounter analysis; AS-S: crystal structure modelling; HB and KF: LCMS and qTOF method sections; XX, DAH, and PPD: writing; DAB: review and editing. All authors read and approved the final version.

Conflict of interest

The authors declare no conflict of interest.

Data availability

All data supporting the findings of this study are available within the paper and within its supplementary data published online.

References

Abe S, Sado A, Tanaka K, et al. 2014. Carlactone is converted to carlactonoic acid by MAX1 in Arabidopsis and its methyl ester can directly interact with AtD14 in vitro. Proceedings of the National Academy of Sciences, USA **111**, 18084–18089.

Alder A, Jamil M, Marzorati M, Bruno M, Vermathen M, Bigler P, Ghisla S, Bouwmeester H, Beyer P, Al-Babili S. 2012. The path from beta-carotene to carlactone, a strigolactone-like plant hormone. Science **335**, 1348–1351.

Arite T, Umehara M, Ishikawa S, Hanada A, Maekawa M, Yamaguchi S, Kyozuka J. 2009. d14, a strigolactone-insensitive mutant of rice, shows an accelerated outgrowth of tillers. Plant & Cell Physiology **50**, 1416–1424.

Arvidsson S, Kwasniewski M, Riaño-Pachón DM, Mueller-Roeber B. 2008. QuantPrime—a flexible tool for reliable high-throughput primer design for quantitative PCR. BMC Bioinformatics **9**, 465.

Baena-González E, Rolland F, Thevelein JM, Sheen J. 2007. A central integrator of transcription networks in plant stress and energy signalling. Nature **448**, 938–942.

Bainbridge K, Sorefan K, Ward S, Leyser O. 2005. Hormonally controlled expression of the Arabidopsis MAX4 shoot branching regulatory gene. The Plant Journal **44**, 569–580.

Bak S, Tax FE, Feldmann KA, Galbraith DW, Feyereisen R. 2001. CYP83B1, a cytochrome P450 at the metabolic branch point in auxin and indole glucosinolate biosynthesis in Arabidopsis. The Plant Cell **13**, 101–111.

Balazadeh S, Siddiqui H, Allu AD, Matallana-Ramirez LP, Caldana C, Mehrnia M, Zanor MI, Kohler B, Mueller-Roeber B. 2010. A gene regulatory network controlled by the NAC transcription factor ANAC092/AtNAC2/ORE1 during salt-promoted senescence. The Plant Journal **62**, 250–264.

Barlier I, Kowalczyk M, Marchant A, Ljung K, Bhalerao R, Bennett M, Sandberg G, Bellini C. 2000. The SUR2 gene of Arabidopsis thaliana encodes the cytochrome P450 CYP83B1, a modulator of auxin homeostasis. Proceedings of the National Academy of Sciences, USA **97**, 14819–14824.

Bläsing OE, Gibon Y, Günther M, Höhne M, Morcuende R, Osuna D, Thimm O, Usadel B, Scheible WR, Stitt M. 2005. Sugars and circadian regulation make major contributions to the global regulation of diurnal gene expression in Arabidopsis. The Plant Cell **17**, 3257–3281.

Booker J, Sieberer T, Wright W, Williamson L, Willett B, Stirnberg P, Turnbull C, Srinivasan M, Goddard P, Leyser O. 2005. MAX1 encodes a cytochrome P450 family member that acts downstream of MAX3/4 to produce a carotenoid-derived branch-inhibiting hormone. Developmental Cell **8**, 443–449.

Brewer PB, Yoneyama K, Filardo F, et al. 2016. LATERAL BRANCHING OXIDOREDUCTASE acts in the final stages of strigolactone biosynthesis in Arabidopsis. Proceedings of the National Academy of Sciences, USA **113**, 6301–6306.

Bu Q, Lv T, Shen H, et al. 2014. Regulation of drought tolerance by the F-box protein MAX2 in Arabidopsis. Plant Physiology **164**, 424–439.

Challis RJ, Hepworth J, Mouchel C, Waites R, Leyser O. 2013. A role for more axillary growth1 (MAX1) in evolutionary diversity in strigolactone signaling upstream of MAX2. Plant Physiology **161**, 1885–1902.

Czechowski T, Stitt M, Altmann T, Udvardi MK, Scheible WR. 2005. Genome-wide identification and testing of superior reference genes for transcript normalization in Arabidopsis. Plant Physiology **139**, 5–17.

de Saint Germain A, Clavé G, Badet-Denisot MA, et al. 2016. An histidine covalent receptor and butenolide complex mediates strigolactone perception. Nature Chemical Biology **12**, 787–794.

Dong L, Miettinen K, Goedbloed M, Verstappen FW, Voster A, Jongsma MA, Memelink J, van der Krol S, Bouwmeester HJ. 2013. Characterization of two geraniol synthases from Valeriana officinalis and Lippia dulcis: similar activity but difference in subcellular localization. Metabolic Engineering **20**, 198–211.

Dvinge H, Bertone P. 2009. HTqPCR: high-throughput analysis and visualization of quantitative real-time PCR data in R. Bioinformatics **25**, 3325–3326.

Fracheboud Y, Luquez V, Björkén L, Sjödin A, Tuominen H, Jansson S. 2009. The control of autumn senescence in European aspen. Plant Physiology **149**, 1982–1991.

Gan S, Amasino RM. 1997. Making sense of senescence (molecular genetic regulation and manipulation of leaf senescence). Plant Physiology **113**, 313–319.

Gao Z, Qian Q, Liu X, Yan M, Feng Q, Dong G, Liu J, Han B. 2009. Dwarf 88, a novel putative esterase gene affecting architecture of rice plant. Plant Molecular Biology **71**, 265–276.

Geiss GK, Bumgarner RE, Birditt B, et al. 2008. Direct multiplexed measurement of gene expression with color-coded probe pairs. Nature Biotechnology **26**, 317–325.

Gomez-Roldan V, Fermas S, Brewer PB, et al. 2008. Strigolactone inhibition of shoot branching. Nature **455**, 189–194.

Grbic V. 2003. SAG2 and SAG12 protein expression in senescing Arabidopsis plants. Physiologia Plantarum **119**, 263–269.

Guo YF, Gan SS. 2006. AtNAP, a NAC family transcription factor, has an important role in leaf senescence. The Plant Journal **46**, 601–612.

Ha CV, Leyva-Gonzalez MA, Osakabe Y, et al. 2014. Positive regulatory role of strigolactone in plant responses to drought and salt stress. Proceedings of the National Academy of Sciences, USA **111**, 851–856.

Hamiaux C, Drummond RS, Janssen BJ, Ledger SE, Cooney JM, Newcomb RD, Snowden KC. 2012. DAD2 is an alpha/beta hydrolase likely to be involved in the perception of the plant branching hormone, strigolactone. Current Biology **22**, 2032–2036.

Hunter DA, Jibran R, Dijkwel P, Chagné D, Sullivan K, Kanojia A, Crowhurst R. 2018. Identification of postharvest senescence regulators

through map-based cloning using detached Arabidopsis inflorescences as a model tissue. In: Guo Y, ed. Plant senescence: methods and protocols. New York: Springer New York, 195–220.

Jiang L, Liu X, Xiong G, et al. 2013. DWARF 53 acts as a repressor of strigolactone signalling in rice. Nature **504**, 401–405.

Jibran R, Sullivan KL, Crowhurst R, Erridge ZA, Chagné D, McLachlan AR, Brummell DA, Dijkwel PP, Hunter DA. 2015. Staying green postharvest: how three mutations in the Arabidopsis chlorophyll b reductase gene NYC1 delay degreening by distinct mechanisms. Journal of Experimental Botany **66**, 6849–6862.

Jing HC, Schippers JH, Hille J, Dijkwel PP. 2005. Ethylene-induced leaf senescence depends on age-related changes and OLD genes in Arabidopsis. Journal of Experimental Botany **56**, 2915–2923.

Kagiyama M, Hirano Y, Mori T, Kim SY, Kyozuka J, Seto Y, Yamaguchi S, Hakoshima T. 2013. Structures of D14 and D14L in the strigolactone and karrikin signaling pathways. Genes to Cells **18**, 147–160.

Kapulnik Y, Delaux PM, Resnick N, et al. 2011. Strigolactones affect lateral root formation and root-hair elongation in Arabidopsis. Planta **233**, 209–216.

Kearse M, Moir R, Wilson A, et al. 2012. Geneious Basic: an integrated and extendable desktop software platform for the organization and analysis of sequence data. Bioinformatics **28**, 1647–1649.

Kim H, Kim HJ, Vu QT, Jung S, McClung CR, Hong S, Nam HG. 2018. Circadian control of ORE1 by PRR9 positively regulates leaf senescence in Arabidopsis. Proceedings of the National Academy of Sciences, USA **115**, 8448–8453.

Kim J, Kim JH, Lyu JI, Woo HR, Lim PO. 2018. New insights into the regulation of leaf senescence in Arabidopsis. Journal of Experimental Botany **69**, 787–799.

Kim JH, Chung KM, Woo HR. 2011. Three positive regulators of leaf senescence in Arabidopsis, ORE1, ORE3 and ORE9, play roles in crosstalk among multiple hormone-mediated senescence pathways. Genes & Genomics **33**, 373–381.

Kim JH, Woo HR, Kim J, Lim PO, Lee IC, Choi SH, Hwang D, Nam HG. 2009. Trifurcate feed-forward regulation of age-dependent cell death involving miR164 in Arabidopsis. Science **323**, 1053–1057.

Kramna B, Prerostova S, Vankova R. 2019. Strigolactones in an experimental context. Plant Growth Regulation **88**, 113–128.

Law SR, Chrobok D, Juvany M, et al. 2018. Darkened leaves use different metabolic strategies for senescence and survival. Plant Physiology **177**, 132–150.

Li GD, Pan LN, Jiang K, Takahashi I, Nakamura H, Xu YW, Asami T, Shen RF. 2016. Strigolactones are involved in sugar signaling to modulate early seedling development in *Arabidopsis*. Plant Biotechnology **33**, 87–97.

Li W, Nishiyama R, Watanabe Y, Van Ha C, Kojima M, An P, Tian L, Tian C, Sakakibara H, Tran LP. 2018. Effects of overproduced ethylene on the contents of other phytohormones and expression of their key biosynthetic genes. Plant Physiology and Biochemistry **128**, 170–177.

Li XF, Li YJ, An YH, Xiong LJ, Shao XH, Wang Y, Sun Y. 2009. AKINbeta1 is involved in the regulation of nitrogen metabolism and sugar signaling in Arabidopsis. Journal of Integrative Plant Biology **51**, 513–520.

Lim PO, Kim HJ, Nam HG. 2007. Leaf senescence. Annual Review of Plant Biology **58**, 115–136.

Liu W, Wu C, Fu Y, Hu G, Si H, Zhu L, Luan W, He Z, Sun Z. 2009. Identification and characterization of HTD2: a novel gene negatively regulating tiller bud outgrowth in rice. Planta **230**, 649–658.

Livak KJ, Schmittgen TD. 2001. Analysis of relative gene expression data using real-time quantitative PCR and the $2^{-\Delta\Delta CT}$ method. Methods **25**, 402–408.

Lv S, Zhang Y, Li C, et al. 2018. Strigolactone-triggered stomatal closure requires hydrogen peroxide synthesis and nitric oxide production in an abscisic acid-independent manner. New Phytologist **217**, 290–304.

Mair A, Pedrotti L, Wurzinger B, et al. 2015. SnRK1-triggered switch of bZIP63 dimerization mediates the low-energy response in plants. eLife **4**, e05828.

Mashiguchi K, Sasaki E, Shimada Y, Nagae M, Ueno K, Nakano T, Yoneyama K, Suzuki Y, Asami T. 2009. Feedback-regulation of strigolactone biosynthetic genes and strigolactone-regulated genes in Arabidopsis. Bioscience, Biotechnology, and Biochemistry **73**, 2460–2465.

McNicholas S, Potterton E, Wilson KS, Noble ME. 2011. Presenting your structures: the CCP4mg molecular-graphics software. Acta Crystallographica. Section D, Biological Crystallography **67**, 386–394.

Otori K, Tamoi M, Tanabe N, Shigeoka S. 2017. Enhancements in sucrose biosynthesis capacity affect shoot branching in Arabidopsis. Bioscience, Biotechnology, and Biochemistry **81**, 1470–1477.

Page T, Griffiths G, Buchanan-Wollaston V. 2001. Molecular and biochemical characterization of postharvest senescence in broccoli. Plant Physiology **125**, 718–727.

Park SY, Yu JW, Park JS, et al. 2007. The senescence-induced staygreen protein regulates chlorophyll degradation. The Plant Cell **19**, 1649–1664.

Rasmussen A, Mason MG, De Cuyper C, et al. 2012. Strigolactones suppress adventitious rooting in Arabidopsis and pea. Plant Physiology **158**, 1976–1987.

Rogers HJ. 2013. From models to ornamentals: how is flower senescence regulated? Plant Molecular Biology **82**, 563–574.

Roy A, Kucukural A, Zhang Y. 2010. I-TASSER: a unified platform for automated protein structure and function prediction. Nature Protocols **5**, 725–738.

Ruyter-Spira C, Kohlen W, Charnikhova T, et al. 2011. Physiological effects of the synthetic strigolactone analog GR24 on root system architecture in Arabidopsis: another belowground role for strigolactones? Plant Physiology **155**, 721–734.

Sakuraba Y, Jeong J, Kang MY, Kim J, Paek NC, Choi G. 2014. Phytochrome-interacting transcription factors PIF4 and PIF5 induce leaf senescence in Arabidopsis. Nature Communications **5**, 4636.

Seto Y, Sado A, Asami K, Hanada A, Umehara M, Akiyama K, Yamaguchi S. 2014. Carlactone is an endogenous biosynthetic precursor for strigolactones. Proceedings of the National Academy of Sciences, USA **111**, 1640–1645.

Seto Y, Yasui R, Kameoka H, et al. 2019. Strigolactone perception and deactivation by a hydrolase receptor DWARF14. Nature Communications **10**, 191.

Song Y, Jiang Y, Kuai B, Li L. 2018. CIRCADIAN CLOCK-ASSOCIATED 1 inhibits leaf senescence in Arabidopsis. Frontiers in Plant Science **9**, 280.

Soundappan I, Bennett T, Morffy N, Liang Y, Stanga JP, Abbas A, Leyser O, Nelson DC. 2015. SMAX1-LIKE/D53 family members enable distinct MAX2-dependent responses to strigolactones and karrikins in Arabidopsis. The Plant Cell **27**, 3143–3159.

Stanga JP, Smith SM, Briggs WR, Nelson DC. 2013. SUPPRESSOR OF MORE AXILLARY GROWTH2 1 controls seed germination and seedling development in Arabidopsis. Plant Physiology **163**, 318–330.

Thomas H. 2013. Senescence, ageing and death of the whole plant. New Phytologist **197**, 696–711.

Tian MQ, Jiang K, Takahashi I, Li GD. 2018. Strigolactone-induced senescence of a bamboo leaf in the dark is alleviated by exogenous sugar. Journal of Pesticide Science **43**, 173–179.

Toh S, Kamiya Y, Kawakami N, Nambara E, McCourt P, Tsuchiya Y. 2012. Thermoinhibition uncovers a role for strigolactones in Arabidopsis seed germination. Plant & Cell Physiology **53**, 107–117.

Trivellini A, Jibran R, Watson LM, O'Donoghue EM, Ferrante A, Sullivan KL, Dijkwel PP, Hunter DA. 2012. Carbon deprivation-driven transcriptome reprogramming in detached developmentally arresting Arabidopsis inflorescences. Plant Physiology **160**, 1357–1372.

Ueda H, Kusaba M. 2015. Strigolactone regulates leaf senescence in concert with ethylene in Arabidopsis. Plant Physiology **169**, 138–147.

Umehara M, Hanada A, Yoshida S, et al. 2008. Inhibition of shoot branching by new terpenoid plant hormones. Nature **455**, 195–200.

Usadel B, Bläsing OE, Gibon Y, Retzlaff K, Höhne M, Günther M, Stitt M. 2008. Global transcript levels respond to small changes of the carbon status during progressive exhaustion of carbohydrates in Arabidopsis rosettes. Plant Physiology **146**, 1834–1861.

Wang L, Wang B, Jiang L, Liu X, Li X, Lu Z, Meng X, Wang Y, Smith SM, Li J. 2015. Strigolactone signaling in arabidopsis regulates shoot development by targeting D53-Like SMXL repressor proteins for ubiquitination and degradation. The Plant Cell **27**, 3128–3142.

Wang Y, Bouwmeester HJ. 2018. Structural diversity in the strigolactones. Journal of Experimental Botany **69**, 2219–2230.

Waters MT, Nelson DC, Scaffidi A, Flematti GR, Sun YK, Dixon KW, Smith SM. 2012. Specialisation within the DWARF14 protein family confers distinct responses to karrikins and strigolactones in Arabidopsis. Development **139**, 1285–1295.

Weaver LM, Amasino RM. 2001. Senescence is induced in individually darkened Arabidopsis leaves, but inhibited in whole darkened plants. Plant Physiology **127**, 876–886.

Yamada Y, Furusawa S, Nagasaka S, Shimomura K, Yamaguchi S, Umehara M. 2014. Strigolactone signaling regulates rice leaf senescence in response to a phosphate deficiency. Planta **240**, 399–408.

Yang J, Yan R, Roy A, Xu D, Poisson J, Zhang Y. 2015. The I-TASSER Suite: protein structure and function prediction. Nature Methods **12**, 7–8.

Yano JK, Wester MR, Schoch GA, Griffin KJ, Stout CD, Johnson EF. 2004. The structure of human microsomal cytochrome P450 3A4 determined by X-ray crystallography to 2.05-Å resolution. Journal of Biological Chemistry **279**, 38091–38094.

Yao R, Ming Z, Yan L, et al. 2016. DWARF14 is a non-canonical hormone receptor for strigolactone. Nature **536**, 469–473.

Yoneyama K, Mori N, Sato T, et al. 2018. Conversion of carlactone to carlactonoic acid is a conserved function of MAX1 homologs in strigolactone biosynthesis. New Phytologist **218**, 1522–1533.

Zhang Y. 2008. I-TASSER server for protein 3D structure prediction. BMC Bioinformatics **9**, 40.

Zhang Y, van Dijk AD, Scaffidi A, et al. 2014. Rice cytochrome P450 MAX1 homologs catalyze distinct steps in strigolactone biosynthesis. Nature Chemical Biology **10**, 1028–1033.

Zhao LH, Zhou XE, Wu ZS, et al. 2013. Crystal structures of two phytohormone signal-transducing α/β hydrolases: karrikin-signaling KAI2 and strigolactone-signaling DWARF14. Cell Research **23**, 436–439.

Zheng K, Wang X, Weighill DA, et al. 2016. Characterization of DWARF14 genes in populus. Scientific Reports **6**, 21593.

Zhou F, Lin Q, Zhu L, et al. 2013. D14-SCF(D3)-dependent degradation of D53 regulates strigolactone signalling. Nature **504**, 406–410.